Campbell, K., Mundy, C. J., Landy, J. C., Delaforge, A., Michel, C., & Rysgaard, S. (2016). Community dynamics of bottom-ice algae in Dease Strait of the Canadian Arctic. *Progress in Oceanography*, *149*, 27-39. https://doi.org/10.1016/j.pocean.2016.10.005

Community dynamics of bottom-ice algae in Dease Strait of the Canadian Arctic

K. Campbell*[1], C.J. Mundy[1], J.C. Landy[1], A. Delaforge[1], C. Michel[1,2] and S. Rysgaard[1,3,4]

[1]*Centre for Earth Observation Science, Faculty of Environment, Earth and Resources, University of Manitoba, Winnipeg, Manitoba, Canada R3T 2N2*

[2] *Freshwater Institute, Fisheries and Oceans Canada, 501 University Crescent, Winnipeg, Manitoba R3T 2N6, Canada*

[3]*Arctic Research Centre, Department of Bioscience, C.F.Møllers Allé 8, 1110, 213, University of Aarhus, 8000 Aarhus C, Denmark*

[4]*Greenland Institute of Natural Resources, Kivioq 2, 3900 Nuuk, Greenland*

** Corresponding author*
Email address: umcampb2@myumanitoba.ca (K. Campbell)

Abstract

Sea ice algae are a characteristic feature in ice-covered seas, contributing a significant fraction of the total primary production in many areas and providing a concentrated food source of high nutritional value to grazers in the spring. Algae respond to physical changes in the sea ice environment by modifying their cellular carbon, nitrogen and pigment content, and by adjusting their photophysiological characteristics. In this study we examined how the ratios of particulate organic carbon (POC) to nitrogen (PON), and POC to chlorophyll *a* (chl *a*), responded to the evolving snow-covered sea ice environment near Cambridge Bay, Nunavut, during spring 2014. We also estimated photosynthesis-irradiance (PI) curves using oxygen-optodes *and* evaluated the resulting time-series of PI parameters under thin and thick snow-covered sites. There were no significant differences in PI parameters between samples from different overlying snow depths, and only the maximum photosynthetic rates in the absence of photoinhibition (P_s^B) and photoacclimation (I_S) parameters changed significantly over the spring bloom. Furthermore, we found that both these parameters increased over time in response to increasing percent transmission of photosynthetically active radiation (T_{PAR}) through the ice, indicating that *light was a limiting factor of photosynthesis* and was an important driver of temporal (over the spring) rather than spatial (between snow depths) variability in photophysiological response. However, we note that spatial variability in primary production was evident. Higher T_{PAR} over the spring and under thin snow affected the composition of algae over both time and space, causing greater POC:chl *a* estimates in late spring and under thin snow cover. Nitrogen limitation was pronounced in this study, likely reducing P_s^B and algal photosynthetic rates, and increasing POC:PON ratios to over

six times the Redfield average. Our results highlight the influence of both light and nutrients on ice algal biomass composition and photophysiology, and suggest a limitation by both resources over a diel period.

Keywords: photoadaptation, sea ice, algology, Arctic zone, oxygen, nutrients

1. Introduction

Sea ice algae are important contributors to the base of the Arctic marine food web. Their abundance in the bottom of sea ice during the spring bloom provides concentrated nutrition for grazers at a time when resources are otherwise limited (Cota et al., 1989 and Legendre et al., 1992). This food source is particularly significant because diatoms that are prevalent in sea ice algal communities contain large amounts of high-energy poly-unsaturated fatty acids (PUFAs) (Leu et al., 2010). Ice algal photosynthetic carbon uptake and oxygen release also significantly affect sea ice carbon dynamics (Brown et al., 2015), thereby influencing air-sea gas exchanges (Else et al., 2012).

For most of the spring the spatial distribution of bottom ice algal biomass (e.g. Campbell et al., 2014a, Mundy et al., 2007 and Rysgaard et al., 2001) and production (e.g. Gosselin et al., 1985, Smith et al., 1988 and Michel et al., 1988) varies in response to light availability that is largely controlled by snow depth. Ice algal chlorophyll *a* (chl *a*) biomass and production are also influenced by other factors that include nutrient availability (Lavoie et al., 2005), species composition (Gosselin et al., 1997) and stability of the ice matrix (Campbell et al., 2014). These factors contribute to the range of biomass and production measurements that are reported in the literature, although, the significance

92 of each changes seasonally with the progression of spring melt and between different
93 study regions (Leu et al., 2015).

94 Ice algae can respond to changing environmental conditions by modifying their
95 cellular carbon and nitrogen composition, as documented by shifts in particulate organic
96 carbon (POC), nitrogen (PON) and chl *a* ratios. On average this results in a ratio of 106
97 mols carbon to 16 mols nitrogen, or 6.6 mols POC:PON, for marine phytoplankton
98 (Miller and Wheeler, 2016). Although, recent studies have suggested a broader range for
99 ice algae from 3 to 24 mol:mol (Niemi and Michel, 2015), where values may increase as
100 a result of acclimation to high light intensities or nutrient limitation (Demers et al., 1989
101 and Gosselin et al., 1990). Particulate carbon to chl *a* ratios typically increase with
102 acclimation to high light and low nutrient conditions (Gosselin et al., 1990 and Michel et
103 al., 1996), resulting in a large range of estimates from 5 to 263 mg:mg for ice algae
104 (Nozais et al., 2001).

105 Ice algae may also adjust the photosynthetic apparatus as seen by changing
106 photosynthetic-irradiance (PI) parameters in response to environmental conditions. For
107 example, PI parameters can vary considerably due to inorganic nutrient availability, the
108 activity of photosynthetic enzymes (Michel et al., 1988), as well as light (Cota and
109 Horne, 1989), salinity (Bates and Cota, 1986) and temperature conditions (Michel et al.,
110 1989). The effects of these often competing or overlapping factors on parameter
111 estimates can make their interpretation complex (Cota and Smith, 1991).

112 The general flow of surface waters in the Canadian Arctic Archipelago is from west
113 to east; however, water in the Coronation Gulf has been suggested to exit both to the
114 Amundsen Gulf in the west and through Dease Strait to the east (McLaughlin et al.,

2004). These suggested patterns of surface currents in the region of Dease Strait near Cambridge Bay, Nunavut, are *largely driven by* the high level of riverine input, and indicate that water at the study site may not readily exchange with neighboring water bodies. These factors have the potential to cause low surface-water exchange with surrounding water bodies that could limit the re-supply of new nutrients to the bottom-ice. Furthermore, low nutrient inflow from the Beaufort Sea in the west could also promote nutrient limited conditions in the region of Dease Strait (Tremblay et al., 2015).

The goal of our study is to investigate the influence of inorganic nutrient availability and light intensity on sea ice algal composition and photosynthetic response over the spring bloom in Dease Strait, Nunavut. To meet this goal, we collected field observations in the region during the Ice Covered Ecosystem - CAMbridge bay Process Study (ICE-CAMPS) between April and June, 2014. Measurements of production from optode incubation methods are used to model PI relationships and derive associated photophysiological parameters for ice algae samples collected under thin and thick snow depths. Coincident measurements of environmental conditions were also recorded to assess potential controls of parameter response.

2. Materials and Methods

2.1 Field Site

Samples were collected in the vicinity of an ice camp established in Dease Strait, Nunavut, Canada (69.03°N, 105.33°W), that was about 5 km offshore from the community of Cambridge Bay. The region is in close proximity to mainland Canada, and receives freshwater inputs from the nearby Coppermine, Hood, Burnside and Ellice rivers

(Fig. 1), with historical average flow rates of 255 (above copper creek), 75.6, 134 and 83.4 $m^3 s^{-1}$ (Environment Canada). Water depth at the station was 60 m and the landfast first-year sea ice in the region was covered by a drifted snowpack for the duration of sampling. Snow depth was categorized as 'thin' (<10 cm, between snow drifts) or 'thick' (15-25 cm, snow drifts). We sampled on 12 occasions between 21 April and 9 June, at approximately 4-day intervals.

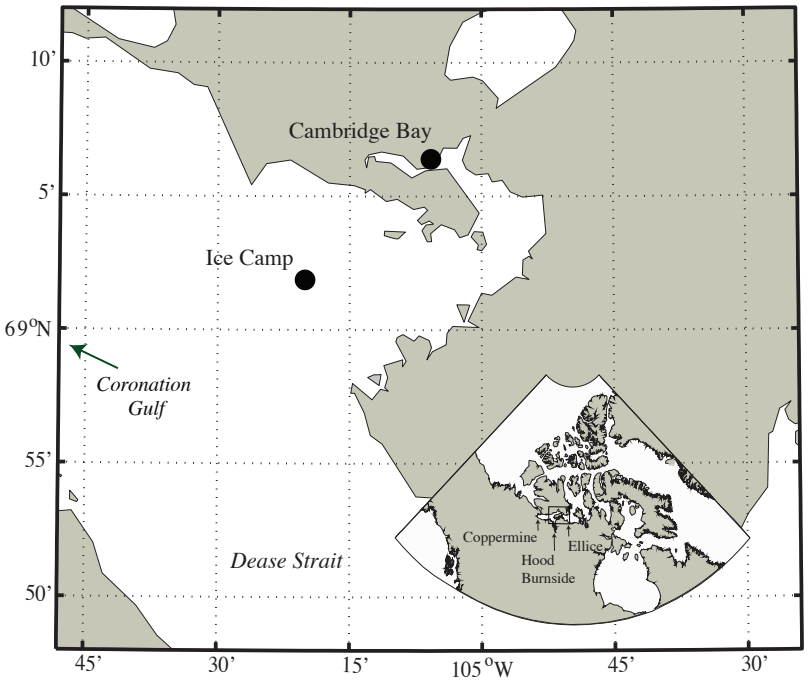

Fig. 1 Map of study location near Cambridge Bay, Nunavut. Inset includes approximate locations of the main rivers in the area.

2.2 Field sampling

Ice cores were collected at newly chosen thin and thick snow sites approximately every four days (one sampling cycle) using a 9 cm *Mark II Kovacs* core barrel. The bottom 0-5 cm of six to eight cores were pooled together for each site, while snow depth and ice thickness for each core were recorded and averaged. A separate core at each snow site was taken for analysis of bulk nutrients.

Average measurements ($n = 3$) of *photosynthetically active radiation (PAR) for surface downwelling and upwelling, as well as* under-ice downwelling were collected opportunistically between 9:00 and 12:30 local time throughout the sample period using 2π quantum sensors (LI-COR) that were calibrated to air and water, respectively. The average of three values was calculated from readings to a *LI-1000* data logger, *and albedo was calculated as the ratio of surface upwelling to downwelling*. The under-ice sensor was deployed approximately 30 cm beneath the ice-ocean interface using a mechanical arm and the protocol described in Campbell et al. (2014b). Transmittance was determined as the percent downwelling PAR transmitted to surface waters under the ice. *Due to irregular collection of transmittance data and the need to perform paired statistical analyses (see Section 2.5), measurements ± 2 days of core collection were averaged to estimate PAR transmittance at the ice core sampling interval of approximately 4 days. Estimates exceeding this 2-day threshold were not included in averaging, resulting in a total of 10 sampling events that are referred to hereafter as PAR transmittance (T_{PAR}).* Finally, daily profiles of conductivity, temperature and depth (CTD) were made of the water column using an RBR XR-620 sensor.

Following transport to laboratory facilities in Cambridge Bay, pooled ice samples were melted in the dark for 24 h in 0.2 μm filtered seawater (FSW) with a mean ± standard deviation of 28 ± 0.3 salinity, that had been collected and filtered 24 h prior to use, which was added at a ratio of three parts FSW to one part ice. This melted sea ice-FSW solution from the pooled cores was used for all incubations and measurements to follow, except for bulk nutrients that were melted separately in the dark without

dilution. To account for FSW dilution when applicable, the volume of each pooled sample were multiplied by the ratio of total volume (FSW + ice melt) to ice melt.

A full core was also taken at the thin snow cover site to measure temperature (Testo 720 probe) and salinity (*Orion Star* A212 conductivity meter) for the bottom 0-5 cm, and 10 cm sections above. These values were used to calculate percent brine volume following the equations of Cox and Weeks (1983).

2.3 Laboratory analysis

2.3.1 Environmental variables

Two subsamples of chl *a* were measured on the melted cores following filtration on GF/F filters (*Whatmann*) and subsequent pigment extraction in 10 ml of 90% acetone for 24 h. Fluorescence was measured before and after acidification with 5% HCl (*Turner Designs Trilogy* Fluorometer) (Parsons et al., 1984) and chl *a* concentration was determined from these measurements using the equations of Holm-Hansen et al. (1965). The salinity of all melted ice samples were measured using an *Orion Star* A212 conductivity meter. A sub-sample of the melted ice-FSW solution was also filtered onto pre-combusted GF/F filters for analysis of POC and PON, and a filter blank was also collected for each sampling event. These samples were kept frozen until measurement on a continuous-flow isotope ratio mass spectrometer (*Thermo Scientific*) following Glaz et al. (2014). Filtrate for nutrient analysis was collected from the undiluted core using sterilized syringe filters and GF/F filters previously combusted at 450°C for 5 h. Samples were frozen for approximately 6 months at -20°C prior to analysis of nitrate (NO_3) and nitrite (NO_2) concentration, together referred to as NO_x, phosphate (PO_4) and silicic acid

199 ($Si(OH)_4$) on an auto analyzer (*Seal Analytical*) (Strickland and Parsons, 1972). *Nutrient*
200 *analysis was also completed on water of the ice-ocean interface that was collected and*
201 *processed on days of ice core collection*.
202
203 *2.3.2 Bacteria production using ^{3}H-Leucine*
204 Bacteria production was determined by incubating 6-15 ml subsamples of the
205 melted ice-FSW solution of pooled cores, with ^{3}H-leucine following Kirchman (2001).
206 Subsamples were dispensed into sterile polycarbonate vials and inoculated with
207 ^{3}H-leucine for a final concentration of 10 nM. Immediately after this step, three of the
208 control vials were fixed with 50% trichloroacetic acid (TCA, final concentration 5%),
209 before the samples were vortexed and incubated at -1.5°C in darkness. Following 6 h
210 incubation, the three remaining active subsamples were fixed with TCA (final
211 concentration 5%) before filtration through 0.2 μm cellulose acetate membranes
212 (*Whatmann*). Filters were rinsed with 5% TCA and 80% ethanol before they were dried
213 in 7 ml scintillation vials, and dissolved by adding 0.5 ml ethyl acetate. The activity of
214 the sample was measured on a liquid scintillation counter (*Hidex Triathler*) after an
215 extraction period of 24 to 48 h in 5 ml of Ecolume scintillation cocktail. The specific
216 activity of the ^{3}H-leucine working solution (SA, dpm mol^{-1}) used in incubations was also
217 recalculated for each sampling cycle.
218 Bacteria production (μmol Leucine l^{-1} h^{-1}) was calculated using the equations of
219 Kirchman (1993) that required: the average activity of test and control filters (dpm), SA
220 (dpm mol^{-1}), incubation time (h), filtered volume (L) and a core dilution factor to account
221 for ice melt in the FSW. Values reported as mass (g C l^{-1} h^{-1}) in this study were further

multiplied by the theoretical conversion factor of 1.5 kg C mol^{-1} used by Ducklow et al. (2003), which estimates the carbon biomass produced relative to ^{3}H-leucine incorporated into cellular protein.

2.3.3 Optode experimental set-up

Optode incubation chambers were designed similar to a photosynthetron (e.g. Babin, 1994), where black and white-diffuse plexiglass was used to create temperature controlled and watertight chambers that were attached to an external water circulator (Fig. 2). Chambers were equipped with 4-500 ml *Wheaton* borosilicate glass bottles that sat on a lip along either side of the false chamber bottom to permit water flow under, as well as above, the incubation bottles. Four holes aligned with the central position of each incubation bottle were also drilled in the incubator lid. Furthermore, chambers were equipped with custom-built stands that housed magnetic stir-plates at each bottle position (Fig. 2), and were positioned equidistant from a *Hiralite* full spectrum Light Emitting Diode (LED). The use of an LED was an important aspect of the optode set-up because it's low heat emission minimized incubation temperature fluctuations.

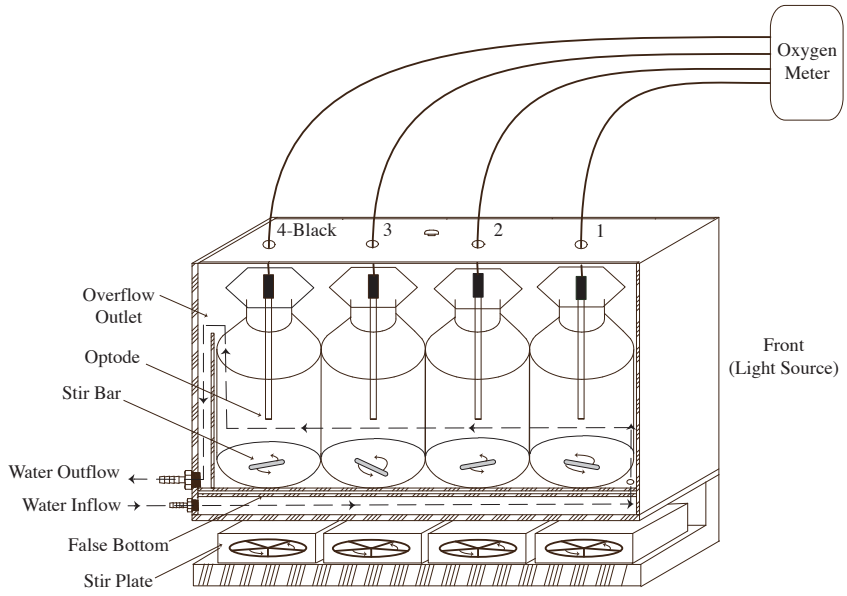

Fig. 2 Illustration of an optode chamber set-up, showing incubation bottle positions 1 (closest to light) through 4-black (furthest from light) and directionality of water flow (dashed arrows).

Continuous measurements of dissolved oxygen were acquired by fitting each incubation bottle with a 10 mm robust *Firesting* optode (*Pyro Science*) with optical insolation that connected to one of two, four-channel *Firesting* optical oxygen meters. Each meter recorded to a single computer using the *Pyro Oxygen Logger* software version 3.0. We positioned each of the sensors in the middle of the sealed incubation bottles by inserting the probes through holes installed in the chamber lid (Fig. 2), as well as through holes drilled in the glass bottle stoppers. It is important to note that the diameter of each stopper hole was nearly equivalent to the 3 mm tip diameter of the optode sensors, ensuring negligible exposure of the sample to air.

The clear bottles were arranged consecutively in the chamber from position one (closest to the light) through three (furthest from the light, Fig. 2), so that samples were incubated at high, medium and low light levels. The average (n = 3) intensity of PAR at

255 these positions was measured immediately following incubations by systematically
256 replacing the oxygen sensors and glass stoppers with a scalar PAR probe (*Walz* model
257 US-SQS/L) that read to a data logger (*LI-COR* LI-1000). The incubation bottle at position
258 four (farthest from the light) was darkened to prevent light from entering.
259
260 *2.3.4 Primary production using optodes*
261 The incubation bottles with magnetic stir bars were filled with the melted ice
262 solution (Section 2.2) using a peristaltic pump, to avoid bubbles being trapped, while the
263 bulk sample was periodically re-suspended. Bottles were overfilled with sample to
264 prevent the formation of a headspace during closure of the glass stopper, and placed into
265 darkened chambers to equilibrate to the set incubation temperature of -1.5°C, that was
266 representative of *in situ* conditions. Optode sensors were calibrated immediately prior to
267 each incubation using 0% and 100% dissolved oxygen standards of 0.17 M sodium
268 dithionite ($Na_2S_2O_4$) and air saturated water, respectively. This was done to account for
269 any sensor drift or photodegradation that may have occurred with extended use
270 (Bagshaw, 2011).
271 Samples were incubated for 70 h under continuous illumination and mixing (1 cm
272 magnet at 60 rpm) while the oxygen concentration was recorded for each bottle at
273 approximately one-second time intervals. Daily temperatures within each chamber were
274 manually recorded (*Traceable* digital thermometer) opportunistically (minimum twice
275 per day) and averaged over the duration of incubations. Due to the volume required to
276 circulate through all incubation chambers, actual incubation temperatures, at -0.66

277 ± 0.25°C, were slightly higher than the desired -1.5°C but remained constant throughout
278 each incubation run.

279 As a result of minor discrepancies in the initial concentration of oxygen between
280 incubation bottles, hourly averages of oxygen concentration in each bottle were made
281 relative to their respective start (T_0) concentrations. Gross primary production
282 ($\mu mol\ O_2\ l^{-1}$) was then calculated for each incubation light intensity as the linear trend of
283 relative oxygen production in illuminated bottles (Fig. 3a, b) plus absolute (linear) black
284 bottle productivity over the entire duration of the experiment. We note that respiration
285 during light conditions may exceed respiration under dark conditions and therefore our
286 gross primary production estimates represent minimum values. Values were converted to
287 milligrams of carbon consumption using the photosynthetic quotient (PQ) of 1.2 (Fenchel
288 and Glud, 2000). All samples incubated in our optode set-up exhibited linear trends of
289 oxygen production (positive or negative) with time, whose slopes were consistently
290 highest in bottle position 1 (high light), followed by bottles 2, 3 and 4 (no light) (Fig. 3).
291 Similar to the trends exhibited in Fig. 3, samples incubated in the dark (bottle 4, Fig. 2)
292 displayed net oxygen consumption for all experiments, represented by negative
293 production.
294

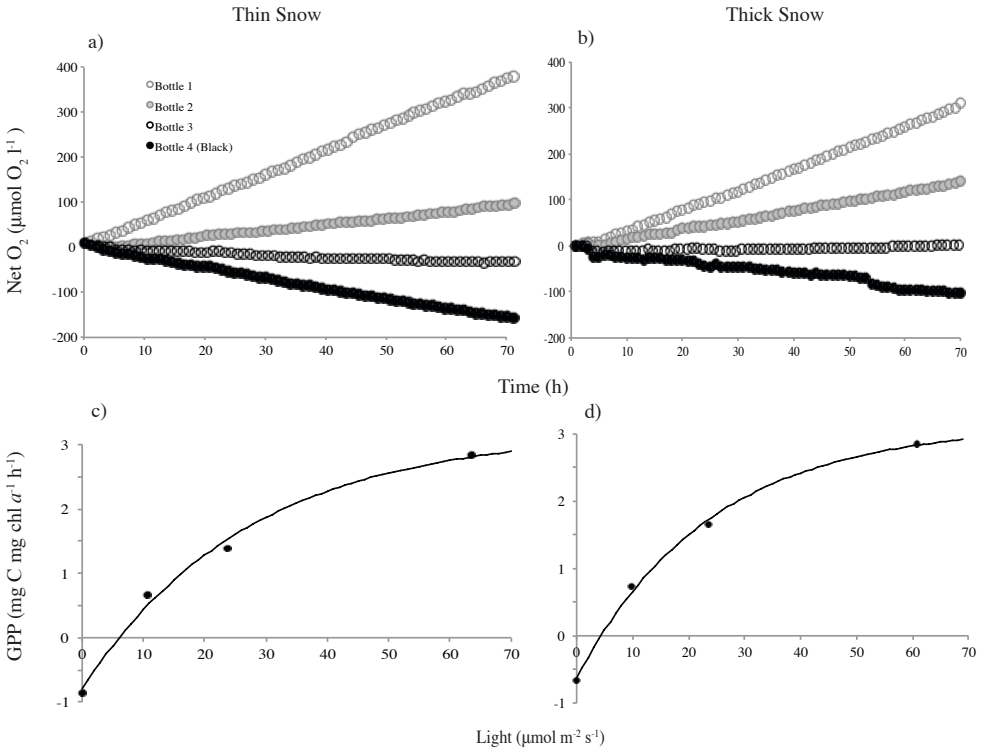

Fig. 3 Examples of community production estimates for thin (a, c) and thick (b, d) snow covers from 22 May. Net change in oxygen per liter during optode incubations is plotted over the 70 h incubation time period for each bottle (a, b). Optode based gross primary production are also plotted as a function of incubation light intensity, relative to chl *a*, with their corresponding exponential models (c, d).

2.4 Fitting photosynthesis-irradiance relationships

Photosynthesis-Irradiance relationships were obtained from the regression of carbon production versus incubation light intensity for each sample cycle. This included primary production of the clear bottles ($n = 3$), as well carbon consumption (negative production) in the dark bottle (Fig. 3c, d). Relationships were calculated using the exponential equation of Platt et al. (1980) without the influence of photoinhibition as it was not observed over the range of experimental irradiances. Photosynthetic parameters were calculated relative to chl *a* biomass and included: P^B_s, maximum photosynthetic rate (mg C mg chl *a* h^{-1}), α^B, photosynthetic efficiency (mg C [mg chl *a*]$^{-1}$ h^{-1} [μ mol photons

311 $m^2\ s^{-1}]^{-1}$), P_0, production at zero irradiance (mg C mg chl *a* h^{-1}), I_c, irradiance where the
312 rate of photosynthesis is balanced by respiration ($I_s = \frac{P_0^B}{\alpha^B}$) (μ mol photons $m^2\ s^{-1}$) and I_s,
313 the photoacclimation parameter ($I_s = \frac{P_s^B}{\alpha^B}$) (μ mol photons $m^2\ s^{-1}$) (Cota and Smith, 1991).
314
315 *2.5 Statistical Analysis*
316 The analytical software SPSS (*IBM* Version 20) was used to perform all statistical
317 analyses in this research for 95% confidence ($p < 0.05$). Student's paired t-tests were run
318 to test differences between thin and thick snow covers. The test statistic (t_n) is reported
319 following these assessments, where *n* indicates the sample size. Pearson correlation
320 statistics (*r*) were calculated to evaluate the significance of linear trends over the spring,
321 and between parameters of interest. All statistics were completed on data for the entire
322 sampling period, unless otherwise specified.
323
324 **3.0 Results**
325 *3.1 Physical characteristics of the field site*
326 Snow thickness (H_S) was relatively constant over the spring sampling period, and
327 averaged 7.5 ± 3.5 and 19 ± 5 cm at thin and thick snow cover sites, respectively (Fig. 4a,
328 b). An exception was the samples collected immediately after a storm on 26 May when
329 snow thickness averaged 18 cm under thin snow and 33 cm under thick snow. These
330 values were not included in the calculated averages of snow depth. Ice thickness (H_I)
331 averaged 1.8 ± 0.10 and 1.7 ± 0.09 m at thin and thick snow cover sites, and increased
332 over the spring from about 1.8 to 2.1 m and 1.75 to 2 m, respectively (Fig. 4a, b). These

differences in snow and ice thickness between sites were significant following a student's paired t-test ($t_{12} = -3.711, p < 0.05$).

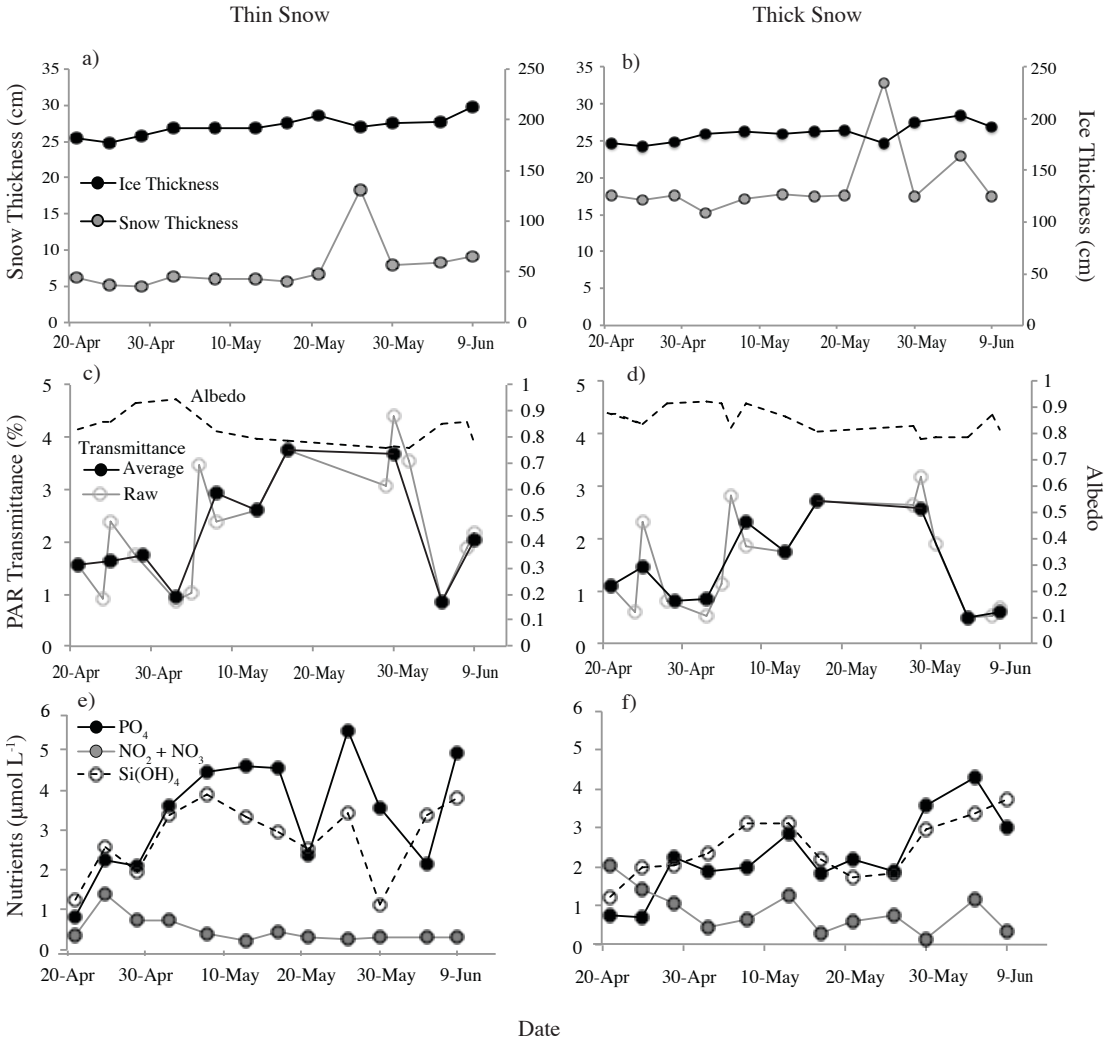

Fig. 4 Site characteristics over the spring sampling period, including snow and ice thickness (a, b), transmittance of photosynthetically active radiation (PAR) *directly measured (Raw) or averaged ± 2 days of core collection (Average)* (c, d), and bottom-ice nutrient concentrations (c, d) under thin (a, c, e) and thick (b, d, f) snow covers. *Albedo measured over thin (c) and thick (d) snow is also shown.*

Snow depth is a dominant control of surface reflectivity prior to melt (Grenfell and Maykut, 1977) and, as a result, the consistency in snow depth for most of the spring corresponds to a largely stable albedo of 0.83 ± 0.06 for thin snow and 0.85 ± 0.05 for

345 *thick snow (Fig. 4c, d). Stable snow depths and albedo indicate the seasonal increase in*
346 *irregularly sampled and averaged PAR transmittance is due to an increasing angle of*
347 *solar elevation, while variability is likely a result of changing weather and cloud*
348 *conditions*.

349 *The percent transmittance of PAR averaged ± 2 days of core collection* (T_{PAR})
350 increased over the spring under thin and thick snow covers from 1.6 and 1.1% on 21
351 April, to 4.4 and 3.2% on 30 May. A storm on 3 June did not affect the depth of snow
352 sampled *as a low site was still found; however, the fresh snow cover and greater depth of*
353 *snow surrounding the site* caused a drop in T_{PAR} on the 5 and 9 June sample dates *that*
354 *represent a period of light conditions in the bottom-ice unique to the rest of the spring. As*
355 *a result, these outliers on* 5 and 9 June *that are uncharacteristic of the seasonal trend*
356 have been removed for all assessments hereafter that include T_{PAR} (see Table 1 of
357 Supplementary Material for additional analyses).

358 Without the outliers after the 3 June storm, the seasonal increase in T_{PAR} was
359 significant at *0.068* % d^{-1} under thin snow ($r^2 = 0.705$, $p < 0.05$) and *0.047* % d^{-1} under
360 thick snow ($r^2 = 0.617$, $p < 0.05$). Light availability at the ice-ocean interface was
361 significantly higher under thin snow cover than thick snow cover ($t_8 = -4.926$, $p < 0.05$),
362 with average T_{PAR} from 21 April to 1 June of 2.2 ± 1%. This corresponds to an averaged
363 transmitted PAR irradiance of 27.4 ± 14.6 μmol photons m^2 s^{-1} over the same time period.
364 In comparison, average T_{PAR} under thick snow cover was 1.7 ± 0.8 % and average
365 transmitted PAR irradiance was 17.7 ± 10.1 μmol photons m^2 s^{-1} (Fig. 4c, d).

366 The bulk concentration of PO_4 and $Si(OH)_4$ in the bottom ice followed similar
367 trends over the spring, but the nature of these relationships differed between snow depths.

Under thin snow, PO_4 and $Si(OH)_4$ displayed a sharper increase at the beginning of the sample period (before 8 May), reaching maximum concentrations of 5.5 μmol L^{-1} and 3.8 μmol L^{-1}, respectively (Fig. 4e). In comparison, PO_4 and $Si(OH)_4$ increased more gradually over the spring under thick snow, to a maximum of approximately 4.3 μmol L^{-1} ($r = 0.799$, $p < 0.05$) and 3.7 μmol L^{-1} ($r = 0.637$, $p < 0.05$), respectively (Fig. 4f). The concentration of NO_x in sea ice decreased initially in the spring under thin and thick snow covers, before remaining under 1 μmol L^{-1} for most of the study period (Fig. 4e, f).

Phosphate concentrations were significantly higher under thin than under thick snow cover ($t_{12} = -2.510$, $p < 0.05$), with averages of 3.41 ± 1.44 μmol L^{-1} and 2.27 ± 1.04 μmol L^{-1}, respectively. The concentration of NO_x was significantly greater under thick snow ($t_{12} = 2.212$, $p < 0.05$) with an average of 0.85 ± 0.51 μmol L^{-1} versus 0.48 ± 0.34 μmol L^{-1} under thin snow. However, there was no significant difference in $Si(OH)_4$ concentration between thin (average 2.79 ± 0.93 μM) and thick (average 2.48 ± 0.77 μM) snow covers ($t_{12} = -1.288$, $p = 0.224$). *Nutrient abundance at the ice-ocean interface did not significantly change over the sampling period (Fig. 5). The average concentration of PO_4, NO_x, $Si(OH)_4$ were 0.84 ± 0.1 μmol L^{-1}, 1.1 ± 0.2 μmol $L^{-1}$and 5.6 ± 0.5 μmol L^{-1}, respectively.*

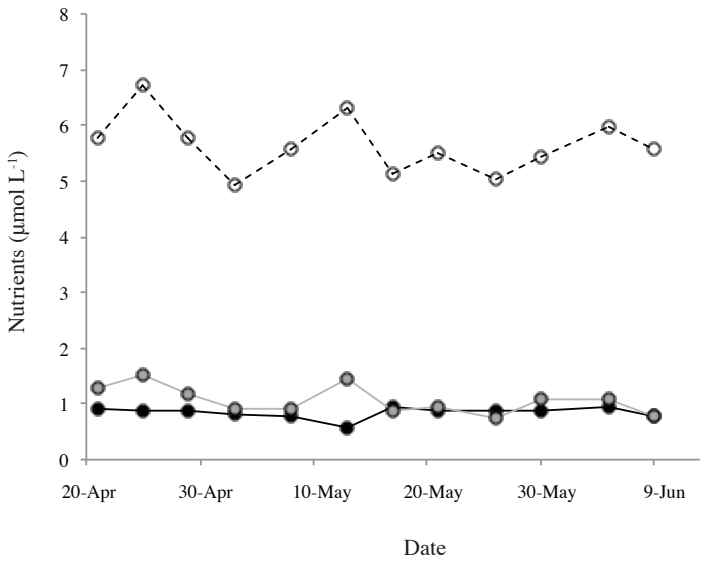

Fig. 5 *Concentration of phosphate (PO_4)(black), nitrate + nitrite (NO_3 + NO_2)(grey) and silicate ($Si(OH)_4$)(white) at the ice-ocean interface over the sampling period.*

The bottom 5 cm of ice salinity remained fairly constant at 8.3 ± 0.6 and brine volume that averaged 29 ± 6%, did not significantly change (p = 0.241) (Fig. 5a). *As a result, the ratio of brine to bulk salinity in the bottom 0-5 cm of sea ice was also stable over the season at 3.1 ± 0.6 (p = 0.516)*. However, seasonal warming drove an increase in brine volume throughout the ice profile over the sampling period (Fig 6b).

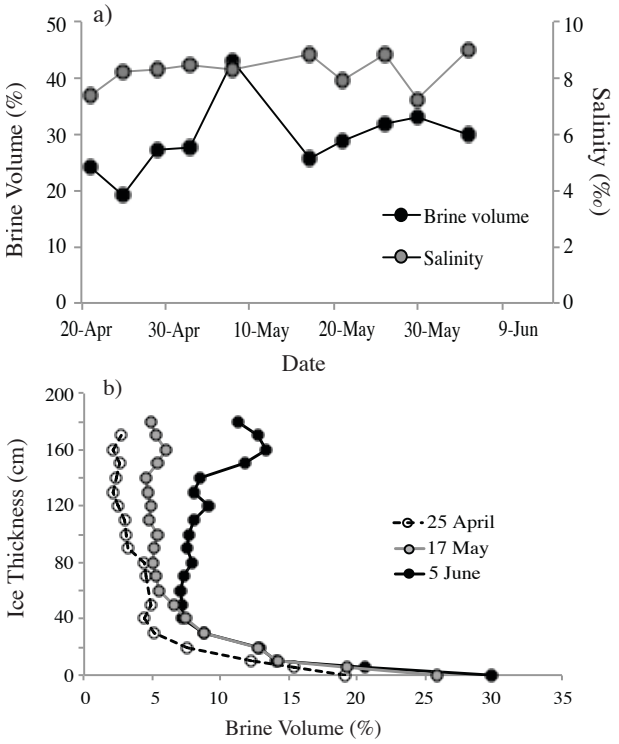

Fig. *6* Bulk salinity and brine volume over the spring sampling period in the bottom 5 cm of sea ice (a) and brine volume profile from the ocean-ice interface (0 cm) to air-ice interface on 17 May, 25 April and 5 June. Values are from ice under thin snow cover.

3.2 Chlorophyll a, carbon and nitrogen

Bottom-ice chl *a* increased over the study from 6.1 to 10.5 mg m^{-2} under thin snow ($r = 0.682, p < 0.05$), and 4.0 to 11.7 mg m^{-2} under thick snow ($r = 0.451, p = 0.141$) (Fig. *7*a). The maximum concentration of bottom-ice chl *a* under thin snow at 10.5 mg m^{-2} occurred on 9 June at end of the time series, while maximum chl *a* under thick snow occurred prior to this date on 30 May. The concentration of chl *a* in the bottom-ice was not statistically different following a student's t-test ($t_{12} = 1.297$, $p = 0.116$) between thin and thick snow covers, with average values of 6.25 ± 3.1 mg m^{-2} and 5.36 ± 3.5 mg m^{-2}, respectively.

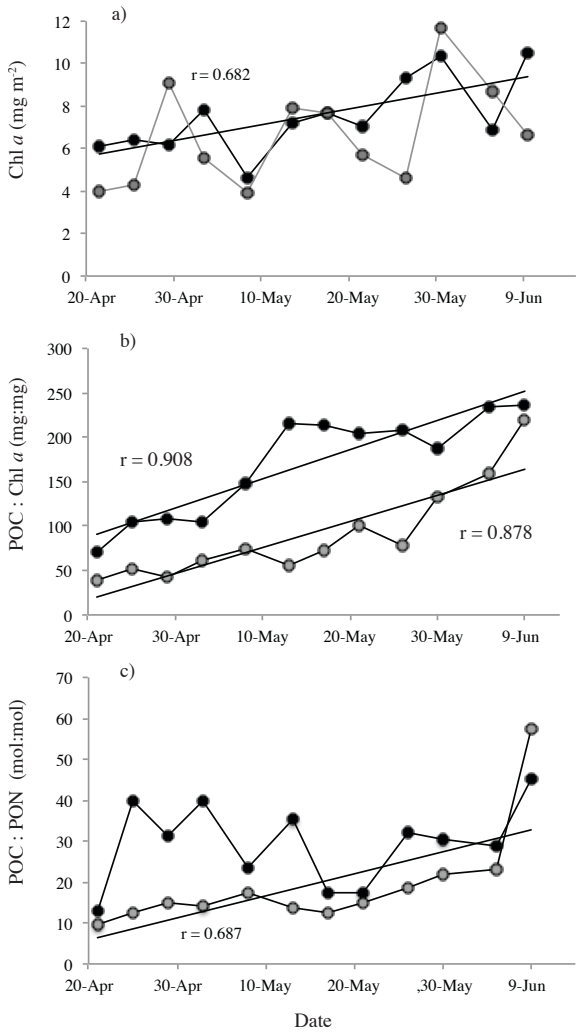

410

411 **Fig. *7*** Seasonal changes in bottom-ice chlorophyll *a* (chl *a*) and the ratios of
412 particulate organic carbon (POC) to chl *a,* and particulate organic nitrogen (PON),
413 under thin (black) and thick (grey) snow covers. Significant (solid line) ($p < 0.05$)
414 seasonal trends are also indicated, with associated correlation coefficients.
415

416 Particulate organic carbon to chl *a* ratios increased linearly over the study from
417 70.2 to 235 (average 169 ± 58.6) under thin snow ($r = 0.908$, $p < 0.05$) and 29.2 to 218.6
418 (averaged 90.3 ± 54) under thick snow ($r = 0.878$, $p < 0.05$) (Fig. 6b). Under thin snow
419 these ratios were highly correlated with T_{PAR} following Pearson correlation analysis,
420 followed by NO_x ($r = -0.619$) and PO_4 ($r = 0.589$) concentrations in the ice (Table 1). The

ratio of POC:chl *a* was also highly correlated with T_{PAR} under thick snow ($r = 0.716$), followed by PO_4 ($r = 0.699$) and $Si(OH)_4$ ($r = 0.697$) concentrations in the ice.

Table 1 Pearson correlation coefficients (top) and *p*-value (bottom) of particulate organic carbon (POC) to chlorophyll *a* (chl *a*) and POC to particulate organic nitrogen (PON) ratios with environmental variables (see text for definitions), for thin and thick snow cover separately and grouped together. Missing data is excluded pairwise and significance ($p < 0.05$) is indicated in bold. The number of observations for each parameter is 12, except for T_{PAR} where the outliers from 5 and 9 June are omitted ($n = 8$).

		Nutrients			Environmental variables			
		PO_4	NO_x	$Si(OH)_4$	Chl *a*	H_I	H_S	T_{PAR}
Thin	POC:chl *a*	**0.589** **0.044**	**-0.619** **0.032**	0.469 0.124	**0.513** **0.088**	**0.796** **0.002**	0.406 0.191	**0.835** **0.01**
	POC: PON	0.374 0.231	0.341 0.279	0.398 0.200	0.448 0.144	0.125 0.698	0.168 0.602	-0.373 0.362
Thick	POC:chl *a*	**0.699** **0.011**	-0.487 0.109	**0.697** **0.012**	0.344 0.274	**0.739** **0.006**	0.090 0.782	**0.716** **0.046**
	POC: PON	0.462 0.130	-0.411 0.184	**0.660** **0.020**	0.158 0.623	0.422 0.172	0.039 0.905	0.474 0.235
Thin & Thick	POC:chl *a*	**0.712** **0**	**-0.612** **0.001**	**0.560** **0.004**	**0.447** **0.029**	**0.809** **0**	0.376 0.070	**0.786** **0**
	POC: PON	**0.510** **0.011**	0.302 0.152	**0.542** **0.006**	0.322 0.124	**0.4017** **0.048**	**0.301** **0**	0.135 0.617

The ratio of POC to PON averaged 29.5 ± 10 under thin snow and did not exhibit any seasonal trend ($r = 0.221$, $p = 0.491$). However, POC:PON under thick snow significantly increased ($r = 0.687$, $p < 0.05$) over the sample period, averaging 19.3 ± 12.7 (Fig. 7c).

Both ratios of POC:chl *a* ($t_{12} = -6.093$, $p < 0.05$) and POC:PON ($t_{12} = -3.158$, $p < 0.05$) were significantly higher under thin than thick snow cover. When combining all data from both snow covers there were significant ($p < 0.05$) correlations between POC:chl *a* with T_{PAR} ($r = 0.786$), PO_4 ($r = 0.712$), NO_x ($r = 0.612$), $Si(OH)_4$ ($r = 0.560$) and chl *a* ($r = 0.447$), and between POC:PON and PO_4 ($r = 0.510$), as well as NO_x ($r = 0.342$) (Table 1).

449 *3.3 Bacterial Production*

450 Bacterial production was not significantly different between thin and thick snow
451 ($t_{12} = -0.318$, $p = 0.757$). Estimates were low throughout the spring and averaged
452 approximately 1 x 10^{-6} ± 6 x 10^{-7} g C l^{-1} h^{-1} over the season for both snow covers (data not
453 shown).

454

455 *3.4 Photosynthesis-Irradiance parameter response*

456 Photosynthesis-irradiance parameters calculated over the sampling period for thin
457 and thick snow are shown in Fig. *8*. The estimates of P^B_s and I_s increased linearly over the
458 spring, which were significant ($p < 0.05$) except for P^B_s under thin snow cover
459 ($p = 0.103$). We note that the estimate of P^B_s on 5 June under thin snow was exceptionally
460 high at 6.7 mg C l^{-1} h^{-1}, and as a result it, along with the derived I_s (72.6 μ mol photons
461 m^{-2} s^{-1}), has not been included in assessments hereafter. The α^B of samples under thin
462 snow appeared to increase until 8 May, after which estimates decreased until the end of
463 sampling on 9 June. This trend was also evident for P_0 under thin and thick snow
464 however, only an exponential decline of α^B under thin snow was significant ($p < 0.05$).
465 Finally, α^B for samples of thick snow cover and all I_c estimates remained constant over
466 the spring and did not significantly change.

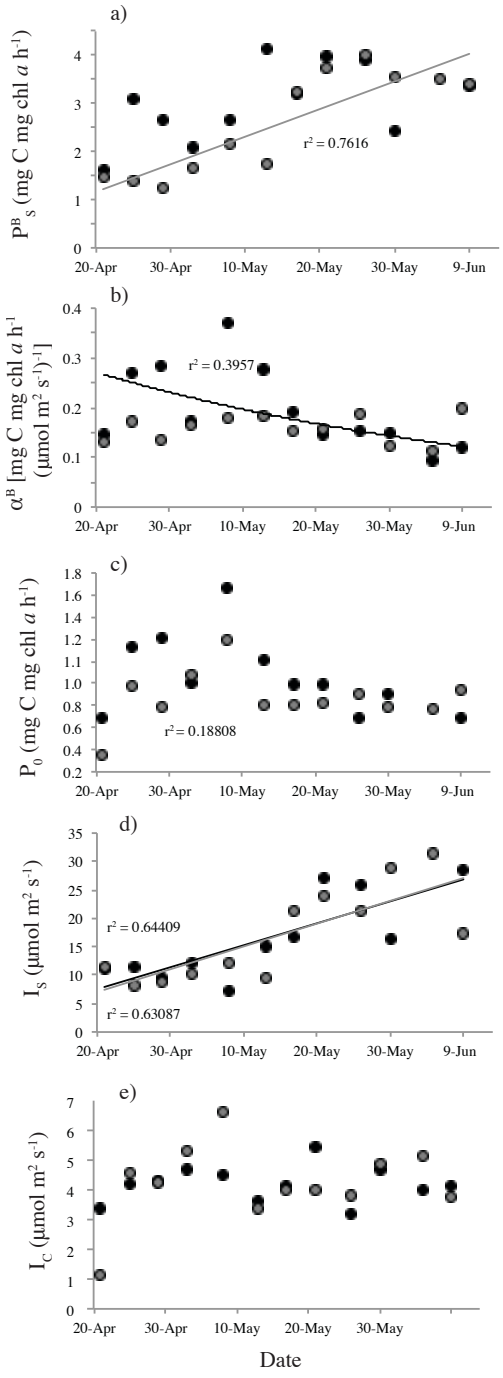

Fig. *8* Photosynthetic parameters P^B_S (a), P_0 (b), α^B (c), I_S (d) and I_C (e) of ice algae under thin (black) and thick (grey) snow covers. Significant (solid line) ($p < 0.05$) seasonal trends are also indicated, with associated correlation coefficients.

The similarity of PI parameter response between snow cover types in Fig. *8* is supported by student's paired t-tests, where parameters from thin and thick snow were not found to be significantly different: P^B_s ($t_{11} = -1.701$, $p = 0.120$), α^B ($t_{12} = -1.740$, $p = 0.110$), P_0 ($t_{12} = -1.875$, $p = 0.088$), I_s ($t_{11} = -0.376$, $p = 0.715$), and I_c ($t_{12} = 0.124$, $p = 0.904$). As a result, PI parameters from thin and thick snow covers have been grouped together for assessments hereafter. Following this grouping of data, only the linear increases in P^B_s ($n = 22$, $r = 0.692$) and I_s ($n = 22$, $r = 0.798$) have significant trends over the sampling period ($p < 0.05$).

The correlations between PI parameters and environmental parameters are summarized in Table 2. The negative correlation between I_s and P_0 ($r = -0.415$) was significant, indicating that the rate of carbon production in darkness, decreased when I_s increased. In addition, P_0 demonstrated a significant positive correlation with the α^B ($r = 0.873$) and I_c ($r = 0.514$).

Table 2 Pearson correlation coefficients (top) and significance (middle) of PI and environmental parameters (see text for definitions) for samples of thin and thick snow covered collectively, except for correlations between I_s and P^B_s or α^B due to co-linearity. Missing data is excluded pairwise and relationships of significance ($p < 0.05$) are been highlighted with bold text. The number of observations for each correlation is also indicated (bottom).

		PI Parameters					Nutrients			Environmental		
		P^B_s	α^B	P_0	I_s	I_c	PO_4	NO_x	$Si(OH)_4$	Chl *a*	H_S	T_{PAR}
PI Parameters	P^B_s		0.1 0.650 23	0.071 0.742 23		0.074 0.736 23	**0.539** **0.008** **23**	**-0.525** **0.01** **23**	0.366 0.085 23	0.270 0.213 23	0.086 0.697 23	**0.661** **0.005** **16**
	α^B			**0.873** **0** **24**		0.042 0.846 24	0.169 0.430 24	-0.004 0.984 24	0.196 0.359 24	-0.382 0.065 24	-0.367 0.078 24	0.232 0.388 16
	P_0				**-0.415** **0.049** **23**	**0.514** **0.010** **24**	0.163 0.447 24	-0.151 0.480 24	0.275 0.193 24	-0.332 0.112 24	-0.359 0.085 24	0.261 0.329 16
	I_s					0.115 0.600 23	**0.439** **0.036** **23**	-0.394 0.063 23	0.236 0.279 23	**0.541** **0.008** **23**	0.307 0.154 23	0.495 0.051 16
	I_c						0.110 0.610	-0.358 0.085	0.259 0.221	0.080 0.709	-0.084 0.696	0.178 0.509

493 The strongest correlation between P^B_s and environmental parameters was T_{PAR}
494 (Table 2), followed by the positive correlation with PO_4 and negative correlation with
495 NO_x concentration. In addition, PO_4 was positively correlated with I_s, which was also
496 correlated with chl *a*.
497
498 **4.0 Discussion**
499 *4.1 Seasonality of nutrients in sea ice*
500 *The availability of nutrients depends on the location of algae in the bottom-ice and*
501 *the resulting proximity to brine or interface water, where the largely sedentary cells can*
502 *only access nutrients in direct contact. The majority of algae in this study were*
503 *concentrated in the bottommost millimeter of ice (pers. observ., Campbell) and, as a*
504 *result, there is uncertainty using bulk measurements from the entire 0-5 cm core section*
505 *to assess nutrient conditions for the algal community. Nevertheless, bulk nutrients*
506 *provide a proxy of nutrient availability in the ice and are used here to assess potential*
507 *nutrient limitation.*
508 The concentrations of PO_4 and $Si(OH)_4$ *in* this study are within the range of 0.26 –
509 5.5 μmol L^{-1} PO_4 (Riedel et al., 2008) and 0.6 – 3.83 μmol L^{-1} $Si(OH)_4$ (Hsaio et al., 1988;
510 Galindo et al., 2014) that are reported for bottom-ice bulk nutrients in the Canadian
511 Arctic during spring. However, NO_x concentrations were considerably lower than that
512 reported elsewhere in the Canadian Arctic during the ice algal bloom (Hsaio et al., 1988
513 and Galindo et al., 2014) *and* are more representative of a nitrogen limited ice
514 environment such as that found in some Greenland fjords at < 2.5 μmol L^{-1} (Mikkelsen
515 et al., 2008; Kaartokallio et al., 2013). *Furthermore, the average NO_x concentration at*

516 *the ice-ocean interface in this study (Fig. 5) is more representative of nitrate*
517 *concentrations in the western Canadian basin's winter surface waters (Tremblay et al.,*
518 *2015) than elsewhere in the Canadian Arctic (Michel et al. 2006). In comparison, the*
519 *average concentrations of PO_4 and $Si(OH)_4$ at the ice interface (Fig. 5) were within*
520 *ranges reported for spring in the Canadian Arctic (Riedel et al., 2008; Rózanksa et al.,*
521 *2009).*

522 Bottom ice nutrients often decrease over the ice algal bloom as nutrient demand
523 surpasses supply (e.g. Lee et al., 2008 and Mikkelsen et al., 2008) from the surface
524 waters (Cota et al., 1987). A decrease in NO_x concentration was observed with increasing
525 chl *a* biomass in this study; however, the concentrations of PO_4 and $Si(OH)_4$ largely
526 increased (Fig. *4*). Positive relationships between nutrient versus chl *a* concentrations
527 have led to the suggestion that ice algae potentially store intracellular nutrients (Cota et
528 al. 1990; Pineault et al. 2013). Indeed a significant positive relationship was observed
529 between PO_4 and chl *a* in our study ($r = 0.605, p < 0.05$).
530
531 *4.2 Nitrogen limitation in Dease Strait*
532 The limited exchange of surface waters in Dease Strait with neighboring water
533 bodies (McLaughlin et al., 2004) suggests that freshwater from ice melt and surrounding
534 rivers (*see* Fig. 1) may accumulate in the region. This process would contribute to the low
535 interface salinities that were observed throughout spring, which averaged 28.1 ± 0.2,
536 compared to elsewhere in the Arctic. Low surface water exchange caused by a more
537 stable halocline would limit the re-supply of new nutrients and lead to depletion of
538 regional nutrient inventories overtime. However, nutrient limitation from stratification of

539 low salinity ice melt and runoff water was present in this study only after 27 May, as
540 indicated by a sharp decrease in salinity of the surface waters in CTD profiles (data not
541 shown). Potential inflow from the Beaufort Sea in the west could also contribute to low
542 salinities and nutrient concentrations observed in the region, as salinities in the surface
543 mixed layer of the Beaufort Sea are relatively fresh at 27-30 (Jackson et al., 2011) and
544 low in nitrogen at 0.1 to 5 μmol L^{-1} (Tremblay et al., 2015).

545 Turbulence in the upper water column enhances the flux of nutrients into the
546 bottom-ice (Cota et al., 1990); however, weak current velocities were observed at the ice
547 interface throughout this study at 2.1 ± 1.2 cm s^{-1} (B. Else pers. comm.). Therefore,
548 mixing to alleviate stratification in late spring and enhance nutrient flux throughout the
549 sampling period was limited. Competition for nutrients between ice algae and
550 phytoplankton was not likely a factor in this study, as chl *a* biomass of sub-ice
551 phytoplankton between the interface and 5 m depth was very low at 0.24 ± 0.01 μg l^{-1}.
552 From this assessment we suggest that the nitrogen limitation in the study area was due to
553 the combined influence of: limited replenishment of new nutrients from surrounding
554 water masses, weak sub-ice turbulence and stratification during late spring.

555

556 *4.3 Light versus nutrient limitation*

557 Low estimates of POC:PON and POC:chl *a* are characteristic of algae that are
558 acclimated to very low light intensities (Harrison et al., 1977, Droop et al., 1982 and
559 Michel et al., 1996), whereas high ratios of POC:PON and POC:chl *a* in ice algae can
560 indicate the presence of nutrient limitation (Demers et al., 1989 and Gosselin et al.,
561 1990). Indeed, lower POC:PON and POC:chl *a* ratios under thick versus thin snow in our

562 study suggest *a greater* influence of light limitation under the thick*er* snow cover. *The*
563 *lower estimates under thick snow also support an inverse relationship between ice algal*
564 *POC:chl a and POC:PON ratios with snow thickness that have been documented*
565 *previously (Arrigo et al., 2013, Niemi and Michel, 2015)*. However, seasonal changes in
566 POC:PON were not correlated with light transmittance (Table 1) and estimates were
567 high, often exceeding the Redfield average of 6.6 and the range of 3 to 24 that has been
568 reported for sea ice in the spring (Gosselin et al., 1990 and Niemi and Michel, 2015).
569 This indicates that nitrogen limitation was *likely* of greater significance than light on
570 POC:PON composition ratios. Further supporting the presence of nitrogen limitation are
571 average bottom-ice molar nutrient ratios of NO_x to PO_4 (N:P) and NO_x to $Si(OH)_4$ (N:Si)
572 that were well below the Redfield composition of phytoplankton at 1.07 N:P and 16 N:Si,
573 at 0.20 ± 0.19 and 0.20 ± 0.15 under thin snow, and 0.62 ± 0.83 and 0.42 ± 0.43 under
574 thick snow, respectively.

575 Particulate carbon to chl *a* ratios reported in this study are within the 5 to 263
576 mg:mg range reported for sea ice by Nozais et al. (2001). The significant positive
577 relationship of POC:chl *a* versus light transmittance suggests the ice algae were
578 acclimating to increasing T_{PAR} over time, where the abundance of chl *a* per cell decreases
579 with increasing bottom-ice light intensity (Gosselin et al., 1990). However, the significant
580 negative relationship between POC:chl *a* and NO_x also suggests an additional influence
581 of nitrogen limitation on the seasonal increase of POC:chl *a* ratios over time, as NO_x
582 limitation should increase with increasing chl *a* biomass and production. These
583 contrasting results support a dual limitation of light and nutrients on ice algal growth. In
584 their ice algal growth model, Lavoie et al. (2005) showed that during night when solar

585 angle is low, light limitation can occur under the snow-covered sea ice, whereas at peak
586 daylight, rapid growth can lead to nutrient limitation due to a finite supply from the water
587 column. Such a condition was expected to occur in our dataset, which was intensified
588 under thick snow covers due to a longer light-limited period over a diel cycle.

589 To evaluate this idea we calculated daily estimates of *in situ* production for thin and
590 thick snow covers using daily-integrated estimates of under-ice PAR (Fig. *9*). Estimates
591 of under-ice PAR *for this analysis* were obtained by applying the average percent
592 transmittance measured at thin (2.2%) and thick (1.7%) sites over the spring (Section
593 3.1), to hourly averaged downwelling surface PAR recorded at a nearby meteorological
594 tower (μmol photons m^{-2} s^{-1}, *Kipp & Zonen PAR-Lite*) on, or within, ± 3 days of ice core
595 extraction dates (except for 21-April as meteorological measurements did not begin until
596 26-April). *From this assessment the average diurnal production was significantly greater*
597 *(t_{11} = 2.389, p = 0.038) under thin snow, which had a higher average production of 15.4*
598 *mg C mg chl a d^{-1} versus 11.1 mg C mg chl a d^{-1} under thick snow (Fig. 9). This supports*
599 *studies that have documented inverse relationships between primary production and*
600 *snow depth as a result of greater light transmission under thin snow cover (Welch and*
601 *Bergmann 1989, Rysgaard et al., 2001)*. The difference in productivity and NO_x
602 concentrations between snow covers also supports our idea that nutrient-limitation of ice
603 algae varies spatially, where higher POC:chl *a*, POC:PON and *in situ* production
604 estimates under thin snow (Fig. *9*) collectively suggest greater NO_x limitation than under
605 thick snow.

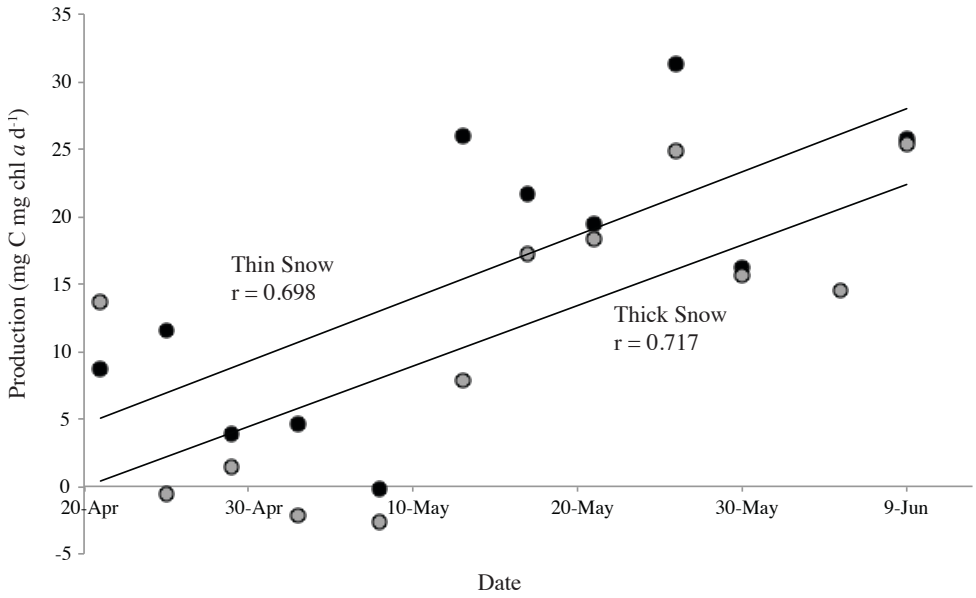

606
607 **Fig. *9*** Estimates of daily-integrated production of sea ice algae under thin (black)
608 and thick (grey) snow covers. Linear trend lines for production over the sampling
609 period are also indicated.
610

611 The bottom-ice algae in this study were predominantly species of diatoms *(pers.*
612 *observ., Campbell)* that *would have been* heavily dependent on silica to form their
613 frustules. The seasonal increase in composition ratios, as a result of changing nitrogen
614 and light conditions, with $Si(OH)_4$ (Table 1), are therefore likely due to coincident
615 increases in silica uptake and subsequent leakage into the bottom-ice environment by
616 diatoms. This explanation may also apply to the significant positive relationships between
617 algal composition and PO_4 (Table 1), as diatoms are known to accumulate intracellular
618 stores of phosphorus under conditions of nitrogen starvation (Harrison et al., 1977).
619

620 *4.4 Measuring photosynthetic-irradiance response using optodes*

621 Published production and photosynthetic parameters of algae have mainly been
622 calculated from ^{14}C-incubations, but measurements of O_2 exchange have also been used
623 (Geider and Osborne, 1992). Both approaches have advantages and limitations, and

624 comparison of ice algal production from these methods has provided variable results (e.g.
625 *McMinn and Hegseth, 2007*, Rysgaard et al., 2001, Glud et al. 2002). A detailed
626 discussion on the strengths and weaknesses of these methods is beyond the scope of this
627 paper. However, we will briefly assess how differences between our optode setup and
628 traditional ^{14}C methods could have influenced parameter estimates, including: incubation
629 time, the maximum light intensity and the use of four data points in the modeling of PI
630 curves.

631 All of the incubations in this study showed linear trends of oxygen production or
632 consumption over the 70 h incubation time (Fig. 3a, b), indicating that factors such as
633 meiofauna consumption of algae and changes in algal physiology that would have
634 produced non-linear responses, were not significant. Low bacterial production in this
635 study (< 4.5% of dark bottle production, Section 3.1) also indicates that error in the
636 calculation of photosynthetic rates from bacterial consumption of oxygen was minimal.

637 The maximum light intensity in optode incubations of approximately 55 μmol
638 photons m^2 s^{-1} was lower than the maximum intensity typically reached in ^{14}C
639 incubations, which can exceed 100 μmol photons m^2 s^{-1} (Michel et al., 1988). The result
640 could have been an underestimate of parameters like P^B_S, if the asymptote was actually
641 reached at stronger irradiances. To assess this potential error we compared our estimates
642 of P^B_S with those modeled during five coincident 3h-^{14}C incubations (following methods
643 of Legendre et al., 1983 and Babin, 1994) that used 10 data points over irradiances up to
644 about 200 μmol photons m^2 s^{-1} (Supplementary Material). We found no significant
645 difference in P^B_S between the methods ($t_9 = -1.032$, $p = 0.332$), indicating that our

646 estimates of maximum photosynthesis were appropriate (Table 2 of Supplementary
647 Material).

648 Finally, to investigate the potential dependence of parameters, particularly α^B, on
649 the use of four data points when estimating PI curves, we fit the ^{14}C data (described
650 above) using only the four data points closest to the average optode incubation light
651 intensities of 0, 10, 21 and 55 μmol m^{-2} s^{-1}. We found that P^B_S and α^B parameters
652 calculated from only four data points were significantly correlated with the full 10 data
653 point estimates ($r > 0.9$, $p < 0.05$), and root mean squared errors were low at 2 mg C mg
654 chl *a* h^{-1} and 0.19 mg C mg chl *a* h^{-1} (μmol m^2 s^{-1})$^{-1}$, respectively (Table 2 of
655 Supplementary Material). This indicates that parameter estimates were not significantly
656 influenced by the number of data points used in our study, because the correlation
657 coefficients would have been much lower if the curves fit from four data points changed
658 considerably. Furthermore, calculation of the standard deviation of optode derived
659 production (i.e., data points on PI curves) was very low, at < 1% of the presented values.

660 *The optode-derived photosynthetic parameters in this study are further supported*
661 *by comparison with estimates that have previously been reported for the Arctic*.
662 *Specifically, all calculated parameters (Fig. 9) are within documented ranges:* P^B_S, *0.007*
663 *- 9.62 mg C [mg chl a]*$^{-1}$ *h*$^{-1}$, α^B, *0.0002 - 2.15 mg C [mg chl a]*$^{-1}$ *h*$^{-1}$ *[μmol photons*
664 *m*$^{-2}$ *s*$^{-1}$*]*$^{-1}$, I_k, *2 - 222 μmol m*$^{-2}$ *s*$^{-1}$ *and* I_c, *0.18 - 7.6 μmol m*$^{-2}$ *s*$^{-1}$ *(Cota, 1985, Gosselin et al., 1985,*
665 *Bates and Cota, 1986, Irwin, 1990)*.
666
667
668

669 4.5 *PI parameters under thin and thick snow cover*

670 There was no statistical difference between the PI parameters of thin and thick
671 snow cover in this study. Therefore, conditions between snow depths were not different
672 enough to cause varied photophysiological responses, particularly given a difference of
673 only 0.5% T_{PAR} between thin and thick snow (see section 3.1). These results suggest that
674 the photoacclimative state of ice algae did not significantly vary with moderate changes
675 (approximately 10 cm) in snow depth in this study. Although, we acknowledge that the
676 movement of snow drifts and resulting unknown snow depth history of sampling sites
677 adds uncertainty to these insights.

678 *Similar to this study, comparable PI responses of algae simultaneously collected*
679 *from ice covered by a range of snow depths have been documented (Cota and Horne,*
680 *1989). However, significant differences in the photophysiological state of ice algae*
681 *following snow removal experiments can occur. For example, higher maximum*
682 *photosynthetic rates (i.e.* P_m^B *or* P_s^B*) and lower* α^B *for algae have been recorded under*
683 *snow-cleared ice compared to snow-covered ice (Cota, 1985, Cota and Horne, 1989). It*
684 *follows that spatial differences in ice algal photophysiology are likely caused by more*
685 *extreme changes in snow cover (i.e. light intensity)y than observed naturally in our study*
686 *area.*

687

688

689

690

691

692 *4.7 Seasonal response of PI parameters to local environmental controls*

693 *4.7.1 Maximum photosynthetic rate*

694 At saturating light intensities above I_s, the maximum rate of photosynthesis is
695 controlled by the rate of carbon fixation and electron transport in the cell. The P^B_m can
696 therefore be summarized as:

697 $$P_m^B = \frac{1}{T} \times N^{PSU} \quad (1)$$

698 where T is the time require for electron transfer between water splitting and CO_2 fixation,
699 and N^{PSU} represents the size of the photosynthetic unit, which includes all catalysts and
700 compounds required for the flow of electrons (Geider and Osborne, 1992). The time of
701 electron transfer increases with light exposure (Barlow et al., 1988) and temperature
702 (Arrigo and Sullivan, 1992), while N^{PSU} increases with the density of photosynthetic
703 reaction centers, electron carriers and pigments (Barlow et al., 1988).

704 It follows that P_m^B or P_s^B could increase over the spring with light intensity (Fig. 4)
705 due to increased electron flow, or the resulting increased availability of products formed
706 in the light reactions of photosynthesis that contribute to N^{PSU} (Barlow et al., 1988).
707 These seasonal responses can explain the increase in P^B_s over the spring that was
708 observed in this study, where the influence of light was particularly important given the
709 significant correlation of P^B_s with T_{PAR} (Table 2). The coincident seasonal increases of P^B_s
710 and T_{PAR} indicate that the potential for primary production is greatest late in the spring
711 owing to relatively high light availability and the photoacclimative state of the ice algae.
712 If ice algae were not capable of changing P^B_s over the spring, light saturation would likely
713 occur at lower intensities and the level of primary production achieved would be smaller.
714 For example, if we apply the estimate of P^B_s from 21 April (early spring) to the daily

production equation and under-ice downwelling intensities of 9 June (late spring), we find a 50% and 70% decrease in primary production under thin and thick snow covers, respectively.

The activity of photosynthetic enzymes is temperature dependent and can also increase P_m^B and P_s^B (Michel et al., 1988 and Arrigo and Sullivan, 1992). However, the bottom-ice environment remained close to freezing temperatures and thus increases in P_s^B with bottom-ice temperature were not significant under thin ($r = 0.216$, $p = 0.577$) or thick snow ($r = 0.173$, $p = 0.632$) in this study. Maximum photosynthetic rates are also affected by nutrient availability, which ensure the elements required to build photosynthetic products are available in the cell (Cota and Horne, 1989). Although the sea ice environment was *affected by* nitrogen *limitation*, the negative correlation between P^B_S and NO_x concentrations indicates that it was not a significant influence (Table 2). These results are in contrast to the positive relationship between nutrient supply and P^B_m reported by Cota and Horne (1989), and instead highlight that light availability was the dominant factor controlling seasonal P^B_s in this study.

4.7.2 Photosynthetic efficiency

At sub-saturating light intensities (i.e. below I_s), algal production is controlled by the rate of light absorption and its conversion to chemical energy. In turn the α^B may be described as:

$$\alpha^B = a^* \times \phi_m \quad (2)$$

where a^* is the chl *a*-specific absorption coefficient, also referred to as the cross sectional absorption, and ϕ_m is the maximum photon yield of photosynthesis that is representative

738 of the mols of oxygen produced or CO_2 consumed by a sample per mol of photons that is
739 absorbed (Geider and Osborne, 1992). From this definition we can see that changes to a^*
740 and, or ϕ_m will affect the photosynthetic efficiency that is measured.

741 One of the greatest influences on a^* is a pigment packaging effect, where
742 absorption of light by chl *a* is lower than the absorption potential of chl *a* in solution
743 (reduced a^*) due to intracellular self-shading. Typically the pigment packaging effect
744 increases with increasing chl *a* per cell, which is a characteristic acclimation strategy of
745 ice algae to low light intensities (Perry et al., 1981 and Gosselin et al., 1990). The ϕ_m is
746 affected by photoprotective mechanisms like the abundance of photoprotective pigments
747 that decrease the amount of absorbed photons used in photosynthesis (decreasing ϕ_m)
748 (Arrigo et al., 2010a), as well as the efficiency of the carboxylation step in photosynthesis
749 (increasing ϕ_m) (Michel et al., 1988 and Arrigo and Sullivan, 1992). As a result of these
750 potentially competing influences, the α^B of algae can increase with *in situ* light intensity
751 (Arrigo et al., 2010a), decrease (Perry et al., 1988), or show no association (Michel et al.,
752 1988).

753 The decrease of α^B under thin snow in this study indicates that ϕ_m could have been
754 reduced from photoprotective mechanisms developed to withstand the greater light
755 intensities of late spring. Although, we note that α^B was not correlated specifically with
756 T_{PAR} ($r = 0.03$, $p = 0.944$), and the melt season that typically brings a large increase in
757 PAR transmission through the ice (Campbell et al., 2015) did not occur. Decreasing NO_x
758 concentrations over the sample period could have also contributed to the decline that was
759 observed (Fig. 4), as nutrient limitation can reduce estimates of α^B (Cota and Horne,
760 1989). However, α^B was also not significantly correlated with ice NO_x concentrations

761 ($r = 0.390$, $p = 0.210$). These findings, in addition to the lack of change in α^B under thick
762 snow, illustrate the complexity of α^B response in sea ice algae and highlight the need for
763 future investigations into the causes of α^B variability.
764
765 *4.7.3 Parameter of photoacclimation*
766 The photoacclimation parameter (I_S) defines the irradiance at which the dominant
767 limitation on production shifts between the efficiency of light harvesting, and the
768 efficiency of carboxylating steps of photosynthesis. The increase in I_S over the spring that
769 was observed in this study (Fig. *8*) has been documented previously for ice algae, and
770 was a result of increasing light intensity (Gosselin et al., 1985). The strong correlation
771 between I_s and T_{PAR} that was observed here supports this conclusion (Table 1).
772
773 *4.7.4 Minimum light for photosynthesis and production in darkness*
774 The P_0 and I_c parameters did not significantly change over the study period,
775 indicating that they were largely independent of the environmental factors that were
776 assessed. For example, it is unlikely that algal respiration changed with the *photo-*
777 *physiological* state of the algae because an increase in P_0 with T_{PAR} over the spring would
778 have been documented. Furthermore, the minimum light intensity required for
779 photosynthesis (I_c) did not change with light exposure or nutrient concentrations over the
780 spring. Although, variability in the I_c parameter between studies in Table 3 suggests
781 further research is needed to determine the potential causes of regional variability, such
782 as dependence of parameters on species composition as well as more simply on the
783 technique used to estimate.

784 The decline of oxygen concentration in black bottles over the duration of all optode
785 experiments (e.g., Fig. 3a, b), rather than zero net change, indicates that respiration by a
786 combination of algae and bacteria was significant in all experiments. The average
787 contribution of ^{3}H-leucine derived bacterial production (BP) was low around 3.5% of P_0
788 under thin snow and 4.5% under thick snow (Fig. 7c), but are within *the* accepted range
789 for sea ice (Søgaard et al., 2010). *Similar to BP (Section 3.3), the contribution of bacteria*
790 *to P_0 was not different between thin and thick snow covers (t_{12} = -1.160, p = 0.271).*
791 *These similarities contrast observations that oxygen consumption from BP typically*
792 *increases with algal activity, as primary production was significantly greater under thin*
793 *snow (Fig. 9) (Smith and Clement, 1990, Ducklow, 2003). It is beyond the scope of this*
794 *study to investigate the dependence of bacteria on snow cover, but our results show that*
795 *photo-stimulus of BP (e.g. Church et al., 2004) that would have occurred under the*
796 *higher light environment of thin snow, was likely not a factor.*
797 Bacterial respiration would have also contributed to production in the dark bottle,
798 but the influence of bacteria is still likely to be much less than algal respiration.
799 Falkowski and Owens (1978) report a possible range of marine phytoplankton respiration
800 from 10 to 41% of maximum algal photosynthesis, which includes the value of 35%
801 measured by Suzuki et al. (1997) for ice algae in the Canadian Archipelago. Our study's
802 P_0:P^B_s ratios all largely fall within this reported range under thin (average 30.8%) or thick
803 (average 30.3%) snow covers. These ratios also decreased over the spring under thin (r^2 =
804 0.369, p = 0.047) and thick snow cover (r^2 = 0.282, p = 0.070), as a result of relatively
805 constant P_0 but increasing P^B_S (Fig. *8*).
806

5. Summary

Oxygen optodes were used in this study to assess changes in the photosynthesis-irradiance response of sea ice algae under thin and thick snow during the spring bloom. Comparison of calculated PI parameters for algae under thin and thick snow covers showed no statistically significant difference. The strongest changes in PI response documented over the spring were significant increases in P^B_s and I_s parameters, which were largely in response to seasonally increasing percent PAR transmittance. These observations highlight that although differences in PAR values *did not appear to be a primary* factor in causing spatial differences in PI parameters from different snow covers, they were *significant* in driving seasonal changes in ice algal photophysiology. Seasonally increasing light intensity was also an important influence on algal physiology, as seen in the increasing ratios of POC:chl *a* over the spring.

Nitrogen limitation was *also* evident in this study from very low NO_x concentrations in sea ice and interface water, low N:P and N:Si ratios and elevated POC:PON ratios throughout the spring. Nitrogen limitation appeared to influence algal PI parameters, likely resulting in a decrease of P^B_s, α^B and I_s. However, a co-limitation by light was evident over a diurnal period as demonstrated by greater production under thin snow compared to that of thick, which in turn led to greater nutrient stress on the ice algae community.

6. Acknowledgements

The authors would like to recognize the support from a Northern Scientific Training Program grant and Natural Sciences and Engineering Research Council of Canada (NSERC) Canadian Graduate Scholarship to KC, Canada Foundation for Innovation (CFI) and the Canada Excellence Research Chair grant to SR, an NSERC Discovery and Northern Research Supplement Grants to CJM, and in-kind support from the Canadian High Arctic Research Station (CHARS). They also wish to thank Drs. Michel Gosselin, Brent Else, John Iacozza, as well as Megan Shields and Marjolaine Blais for their support. This work represents a contribution to the research programs of ArcticNet, the Arctic Science Partnership (ASP) and the Canada Excellence Research Chair unit at the Centre for Earth Observation Science (CEOS) at the University of Manitoba.

References

Arrigo, K.R., Brown, Z.W., Mills, M.M., 2013. Sea ice algal biomass and physiology in the Amundsen Sea, Antarctica. Elementa: Science of the Anthropocene 2. doi: 10.12952/journal.elementa.000028.

Arrigo, K.R., Mills, M.M., Kropuenske, L.R., van Dijken, G.L., Alderkamp, A.-C., Robinson, D.H., 2010a. Photophysiology in two major southern ocean phytoplankton taxa: Photosynthesis and growth of *Phaeocystis Antarctica* and *Fragilariopsis cylindrus* under different irradiance levels. Integ. Comp. Biol. 50(6), 950-966.

Arrigo, K.R., Mock, T., Lizotte, M., 2010b. Primary Producers and Sea Ice. In: Thomas, D.N., Dieckmann, G.S. (eds) Sea Ice 2nd Ed. Wiley Blackwell Publishing, Malaysia, 283-325.

Arrigo, K.R., Sullivan, C.W., 1992. The influence of salinity and temperature covariation on the photophysiological characteristics of Antarctic sea ice microalgae. J. Phycol. 28, 746-756.

Babin, M., 1994. An incubator designed for extensive and sensitive measurements of phytoplankton photosynthetic parameters. Limnol. Oceanogr. 39(3), 694-702.

Bagshaw, E.A., Wadham, J.L., Mowlem, M., Tranter, M., Eveness, J., Fountain, A.G., Telling, J., 2011. Determination of dissolved oxygen in the Cryosphere: A comprehensive laboratory and field evaluation of fiber optic sensors. Environ. Sci. Technol 45, 700-705.

Barlow, R.G., Gosselin, M., Legendre, L., Therriault, J.-C., Demers, S., Mantoura, R.F.C., Llewellyn, C.A., 1988. Photoadaptive strategies in sea ice microalgae. Mar. Ecol. Prog. Ser. 45, 145-152.

Bates, S.S., Cota, G.F., 1986. Fluorescence induction and photosynthetic responses of Arctic ice algae to sample treatment and salinity. J. Phycol. 22, 421-429.

Brown, K.A., Miller, L.A., Mundy, C.J., Papakyriakou, T., Francois, R., Gosselin, M., Carnat, C., Swystun, K., Tortell, P.D., 2015. Inorganic carbon system dynamics in landfast Arctic sea ice during the early-melt period. J. Geophys. Res. Oceans 120, 3542-3566. doi:10.1002/2014JC010620.

Campbell, K., Mundy, C.J., Barber, D.G., Gosselin, M., 2014. Remote estimates of ice algae biomass and their response to environmental conditions during spring melt. Arctic 67, 375-387. doi.org/10.14430/arctic4409.

Campbell, K., Mundy, C.J., Barber, D.G., Gosselin, M., 2015. Characterizing the sea ice algae chlorophyll a–snow depth relationship over Arctic spring melt using transmitted irradiance. J. Mar. Syst. 147, 76-84.

Church, M.J.H., Ducklow, W., Karl, D.M., 2004. Light dependence of [3H] leucine incorporation in the oligotrophic North Pacific Ocean. Appl. Environ. Microbiol. 70, 4079-4087.

Cota, G.F., 1985. Photoadaptation of high Arctic ice algae. Lett. Nature 315, 219-222.

Cota, G., Anning, J., Harris, L., Harrison, W., Smith, R.E.H., 1990. Impact of ice algae on inorganic nutrients in seawater and sea ice in Barrow Strait, N.W.T, during spring. Can. J. Aquat. Sci. 47(7), 1402-1415.

Cota, G., Horne, E., 1989. Physical control of arctic ice algal production. Mar. Ecol. Prog. Ser. 52, 111-121.

Cota G.F., Prinsenberg, S.J., Bennett, E.B., Loder, J.W., Lewis, M.R., Anning, J.L., Watson, N.H.F., Harris, L.R., 1987. Nutrient fluxes during extended blooms of Arctic ice algae. J. Geophys. Res. 92(C2), 1951-1962.

Cota, G., Smith, R.E.H., 1991. Ecology of bottom ice algae: III. Comparative physiology. J. Mar. Syst. 2, 297-315.

Cox, G.F.N., Weeks, W.F., 1983. Equations for determining the gas and brine volumes of in sea-ice samples. J. Glaciol. 29, 306-316.

Demers, S., Legendre, L., Maestrini, S.Y., Rochet, M., Ingram, R.G., 1989. Nitrogenous nutrition of sea-ice microalgae. Polar Biol. 9, 377-383.

Droop, M.R., Mickelson, M.J., Scott, J.M., Turner, M.F., 1982. Light and nutrient status of algal cells. J. Mar. Biol. Assoc. U.K. 62, 403-434.

Ducklow, H.W., 2003. Seasonal production and bacterial utilization of DOC in the Ross Sea, Antarctica. Biogeochem. Ross Sea, 143-157.

Else, B.G.T., Papakyriakou, T.N., Galley, R.J., Mucci, A., Gosselin. M., Miller, L.A., Shadwick, E.H., Thomas, H., 2012. Annual cycles of $pCO2_{sw}$ in the southeastern Beaufort Sea: New understandings of air-sea CO2 exchange in arctic polynya regions. J. Geophys. Res. 117, G00G13. doi:10.1029/2011JC007346.

Environment Canada. Water Office Historical Hydrometric Data. Web. 21 May, 2016. < http://wateroffice.ec.gc.ca>.

Falkowski, P.G., Owens, T.G., 1978. Effects of Light Intensity on Photosynthesis and Dark Respiration in Six Species of Marine Phytoplankton. Mar. Biol. 45, 289-295.

Fenchel, T., Glud, R.N., 2000. Benthic primary production and O_2-CO_2 dynamics in a shallow-water sediment: Spatial and temporal heterogeneity. Ophelia 52(2), 159-171. doi: 10.1080/00785236.2000.10409446.

Galindo, V., Levasseur, M., Mundy, C.J., Gosselin, M., Tremblay, J.-E., Scarratt, M., Gratton, Y., Papakiriakou, T., Poulin, M., Lizotte, L., 2014. Biological and physical processes influencing sea ice, under-ice algae and dimethylsulfoniopropionate during spring in the Canadian Arctic Archipelago. J. Geophys. Res. Oceans 119. doi:10.1002/2013JC009497.

Geider, R.J., Osborne, B.A., 1992. Algal photosynthesis: The measurements of algal gas exchange, Current phycology 2. Springer Science.

Glaz, P., Sirois, P., Archambault, P., Nozais, C., 2014. Impact of forest harvesting on trophic structure of Eastern Canadian Boreal Shield Lakes, Insights from stable isotope analysis. PLoS ONE 9(4), e96143. doi:10.1371/journal.pone.0096143.

Glud, R.N., Rysgaard, S., Kühl, M., 2002. A laboratory study on O_2 dynamics and photosynthesis in ice algal communities:quantification by microsensors, O_2 exchange rates, ^{14}C incubations and a PAM fluorometer. Aquat. Microbiol. Ecol. 27, 301-311.

Gosselin, M., Legendre, L., Therriault, J.-C., Demers, S., 1990. Light and nutrient limitation of sea-ice microalgae (Hudson Bay, Canadian Arctic). J. Phycol. 26, 220-232.

Gosselin, M., Legendre, L., Demers, S., Ingram, R.G., 1985. Responses of sea-ice microalgae to climatic and fortnightly tidal energy inputs (Manitounuk Sound, Judson Bay). Can. J. Fish. Aquat. Sci. 42, 999-1006.

Gosselin, M., Legendre, L., Therriault, J.-C., Demers, S., 1990. Light and nutrient limitations of sea-ice microalgae (Hudson Bay, Canadian Arctic). J. Phycol. 26, 220-232.

Gosselin, M., Levasseur, M., Patricia, A.W., Horner, R.A., Booth, B.C., 1997. New measurements of phytoplankton and ice algal production in the Arctic Ocean. Deep-Sea Res. 44(8), 1623-1644.

Grenfell, T.C., Maykut, G.A., 1977. The optical properties of ice and snow in the Arctic basin. J. Glaciology 18(80), 445-463.

Harrison, P.J., Conway, H.L., Holmes, R.W., Davis, C.O., 1977. Marine diatoms grown in chemostats under silicate or Ammonium limitation III, Cellular chemical composition and morphology of *Chaetoceros debilis*, *Skeletonema costatum* and *Thalassiosira gravida*. Mar Biol Berlin 43, 19-31.

Holm-Hansen, O., Lorenzen, J., Holmes, R.W., Strickland, J.D., 1965. Fluorometric determination of chlorophyll. ICES J. Mar. Sci. 30, 3-15. doi:10.1093/icesjms/30.1.3.

Hsaio, S.I.C., 1988. Spatial and seasonal variations in primary production of sea ice microalgae and phytoplankton in Frobisher Bay, Arctic Canada. Mar. Ecol. Progr. Ser. 44, 275-285.

Irwin, B.D., 1990. Primary production of ice algae on a seasonally-ice-covered continental shelf. Polar Biol. 10, 247-254.

Jackson, J.M., Allen, S.E., McLaughlin, F.A., Woodgate, R.A., Carmack, E.C., 2011. Changes to the near surface waters in the Canada Basin, Arctic Ocean from 1993–2009: A basin in transition. J. Geophys. Res. 116, C10008. doi:10.1029/2011JC007069.

Kaartokallio, H., Søgaard, D.H., Norman, L., Rysgaard, S., Tison, J.L., Delille, B., Thomas, D.N., 2013. Short-term variability in bacterial abundance, cell properties, and incorporation of leucine and thymidine in subarctic sea ice. Aquat. Microbiol. Ecol, 71, 57-73.

Kirchman, D.L., 1993. Chapter 58: Leucine incorporation as a measure of biomass production by heterotrophic bacteria. In: Handbook of Methods in Aquatic Microbial Ecology, 509-518.

Kirchmann, D., 2001. Chapter 12: Measuring bacterial biomass production and growth rates from leucine incorporation in natural aquatic environments. In: Methods in Microbiology 30, 227-237.

Lavoie, D., Denman, K., Michel, C., 2005. Modeling ice algal growth and decline in a seasonally ice-covered region of the Arctic (Resolute Passage, Canadian Archipelago). J Geophys, Res, 110, C11009.

Lee, S.H., Whiteledge, T.E., Kang, S.-H., 2008. Spring time production of bottom ice algae in the landfast sea ice zone at Barrow Alaska. J. Exp. Mar. Biol. Ecol. 367, 204-212.

Legendre, L., Ackley, S.F., Dieckmann, G.S., Gullicksen, B., Horner, R., Hoshiai, T., Melnikov, I.A., Reeburgh, W.S., Spindler, M., Sullivan, C.W., 1992. Ecology of sea ice biota: Part 2 Global significance. Polar Biol. 12, 429–444.

Legendre, L., Demers, S., Yentsch, C.M., Yentsch, C.S., 1983. The 14C method: patterns of dark CO2 fixation and DCMU correction to replace the dark bottle. Limnol. Oceanogr. 28, 996-1003.

Leu, E., Mundy, C.J., Assmy, A., Campbell, K., Gabrielsen, T.M., Gosselin, M., Juul-Pedersen, T., Gradinger, R., 2015. Arctic spring awakening – Steering principles behind the phenology of vernal ice algae blooms. Prog. Oceanogr. 139, 151-170.

Leu, E., Wiktor, J., Soreide, J.E., Berge, J., Falk-Peterson, S., Berge, J., 2010. Increased irradiance reduces food quality of ice algae. Mar. Ecol. Prog. Ser. 411, 49-60. doi:10.3354/meps08647.

Lewis, M.R., Smith, J.C., 1983. A small volume, short incubation time method for the measurement of photosynthesis as a function of incident irradiance. Mar. Ecol. Prog. Ser., 13, 99-102.

McLaughlin, F.A., Carmack, E.C., Ingram, R.G., Williams, W.J., Michel, C., 2004. Oceanography of the Northwest Passage. In: Robinson, A.R., Brink, K.H. (eds), The Sea. President and Fellows of Harvard College, 1211-1242.

McMinn, A., Hegseth, E.N., 2007. Sea ice primary productivity in the northern Barents Sea, spring 2004. Polar Biol. 30, 289-294.

Michel, C., Ingram, R.G., Harris, L.R., 2006. Variability in oceanographic and ecological processes in the Canadian Arctic Archipelago. Prog. Oceanog. 71, 379-401.

Michel, C., Legendre, L., Demers, S., Therriault, J.-C., 1988. Photoadaptation of sea-ice microalgae in springtime: photosynthesis and carboxylating enzymes. Mar. Ecol. Progr. Ser. 50, 177-185.

Michel, C., Legendre, L., Ingram, R.G., Gosselin, M., Levasseur, M., 1996. Carbon budget of sea-ice algae in spring: Evidence of significant transfer to zooplankton grazers. J. Geophys. Res. 101(C8), 18345-18360.

Michel, C., Legendre, L., Therriault, J.-C., Demers, S., 1989. Photosynthetic responses of Arctic sea-ice microalgae to short-term temperature acclimation. Polar Biol. 9, 437-442.

Mikkelson, D.M., Rysgaard, S., Glud, R.N., 2008. Microalgal composition and primary production in Arctic sea ice: a seasonal study from Kobbefjord (Kangerluarsunnguaq), west Greenland. Mar. Ecol. Prog. Ser. 368, 65-74.

Miller, C.B.,Wheeler, P.A., 2012. Biological Oceanography.Wiley Blackwell Publishing, Malaysia.

Mundy, C.J., Barber, D.G., Michel, C., Marsden, R.F., 2007. Linking ice structure and microscale variability of algal biomass in Arctic first-year sea ice using an in situ photographic technique. Polar Biol. 30, 1099-1114.

Niemi, A., Michel, C., 2015. Temporal and spatial variability in sea-ice carbon:nitrogen ration on Canadian Arctic shelves. Elementa: Sci. Anthro. 3(000078). doi:10.12952/journal.elementa.000078.

Nozais, C., Gosselin, M., Michel, C., Tita, G., 2001. Abundance, biomass, composition and grazing impact of the sea-ice meiofauna in the North Water, northern Baffin Bay. Mar. Ecol. Prog. Ser. 217, 235-250.

Parsons, T.R., Maita, Y., Lalli, C.M., 1984. Manual of chemical and biological methods for seawater analysis. Pergamon Press, New York.

Perry, M.J., Talbot, M.C., Alberte, R.S., 1988. Photoadaptation in marine phytoplankton: response of the photosynthetic unit. Mar. Biol. 62, 91-101.

Pineault, S., Tremblay, J.-E., Gosselin, M., Thomas, H., Shadwick, E., 2013. The isotopic signature of particulate organic C and N in bottom ice: Key influencing factors and applications for tracing the fate of ice-algae in the Arctic Ocean. J. Geophys. Res. Oceans 118, 287–300. doi:10.1029/2012JC008331

Platt, T., Gallegos, C.L., Harrison, W.G., 1980. Photoinhibition of photosynthesis in

natural assemblages of marine phytoplankton. J. Mar. Res. 38, 687–701.

Riedel, A., Michel, C., Gosselin, G., LeBlanc, B., 2008. Winter-spring dynamics in sea-ice carbon cycling in the coastal Arctic. J. Mar. Syst. 74, 918-932.

Rózanksa, M., Gosselin, M., Poulin, M., Wiktor, J.M., Michel, C., 2009. Influence of environmental factors on the development of bottom ice protist communities during the winter-spring transition. Mar. Ecol. Progr. Ser. 386, 43-59.

Rysgaard, S., Kuhl, M., Hansen, J.W., 2001. Biomass, production and horizontal patchiness of sea ice microalgae in a high-Arctic fjord (Young Sound, NE Greenland). Mar. Ecol. Prog. Ser. 223, 15-26.

Smith, R.E.H., Clement, P., 1990. Heterotrophic activity and bacterial productivity in assemblages in microbes from sea ice in the High Arctic. Polar Biol. 10, 351-357.

Smith, R.E.H., Anning, J., Clement, P., Cota, G., 1988. Abundance and production of ice algae in Resolute Passage, Canadian Arctic. Mar. Ecol. Progr. Ser. 48, 251-263.

Søgaard, D.H., Kristensen, M., Rysgaard, S., Glud, R.N., Hansen, P.J., Hilligsoe, K.M., 2010. Autotrophic and heterotrophic activity in Arctic first-year sea ice: seasonal study from Malene Bight, SW Greenland. Mar. Ecol. Progr. Ser. 419, 31-45.

Strickland, J.D., Parsons, T.R., 1972. A practical handbook of seawater analysis, 2nd edn. Bull. Fish. Res. Bd. Can.

Suzuki, Y., Kudoh, S., Takahashi, M., 1997. Photosynthetic and respiratory characteristics of an Arctic algal community living in low light and temperature conditions. J. Mar. Syst. 11, 111-121.

Tremblay, J., Anderson, L.G., Matrai, P., Coupel, P., Bélanger, S., Michel, C., Reigstad,

M., 2015. Global and regional drivers of nutrient supply, primary production and CO2 drawdown in the changing Arctic Ocean. Progr. Oceanog. 139, 171-196.

Welch, H.E., Bergmann, M.A., 1989. Seasonal development of ice algae and its prediction from environmental factors near Resolute, N.W.T., Canada. Can. J. Fish. Aquat. Sci. (46), 1793 – 1804.